Food chain chaos due to transcritical point

Bo Deng[a] and Gwendolen Hines[b]
Department of Mathematics and Statistics, University of Nebraska–Lincoln, Lincoln, Nebraska 68588

(Received 8 July 2002; accepted 30 March 2003; published 21 May 2003)

Chaotic dynamics of a classical prey-predator-superpredator ecological model are considered. Although much is known about the behavior of the model numerically, very few results have been proven analytically. A new analytical result is obtained. It is demonstrated that there exists a subset on which a singular Poincaré map generated by the model is conjugate to the shift map on two symbols. The existence of such a Poincaré map is due to two conditions: the assumption that each species has its own time scale ranging from fast for the prey to slow for the superpredator, and the existence of transcritical points, leading to the classical mathematical phenomenon of Pontryagin's delay of loss of stability. This chaos generating mechanism is new, neither suspected in abstract form nor recognized in numerical experiments in the literature. © *2003 American Institute of Physics.* [DOI: 10.1063/1.1576531]

Ecological systems consisting of multiple food chains and webs are extremely difficult to analyze. The role of chaos in ecology is poorly understood. One approach to gain a better understanding on ecological chaos is by studying it in mathematical models of basic food chains of length 3. In this paper we investigate a new chaos generating mechanism in a basic food chain model and determine the ecological parameter ranges in which this type of chaos occurs.

I. INTRODUCTION

The logistic map for population dynamics[1] was one of very few examples of chaos in the early development of chaos theory. The role of chaos in ecology however is hotly debated to this day.[2–4] On one hand, there is little unequivocal evidence that chaos exists in nature,[3] although its existence in laboratory populations has been proved beyond doubt.[5] On the other hand, mathematical models of food chains are rich with chaos. Food chain model chaos was first exhibited in Ref. 6 in 1978, and food web model chaos in Ref. 7 in 1979. Attractors of these early models looked rather similar to the Rössler attractor.[8]

More than a decade later, a rather distinctive chaotic attractor—referred to as tea-cup attractor—was found in a food chain model by Ref. 9. This finding had the effect of accelerating the search for chaos in food chain models. A Rössler-type chaotic attractor was shown numerically to exist in a chemostat food chain model by Ref. 10. A food chain attractor containing a Shilnikov homoclinic orbit[11] was found in Ref. 12 and one containing a degenerate Shilnikov orbit in Ref. 13, see also Ref. 14. The search for field chaos however seemed to be more elusive than ever.[3] It is a prevailing view today among some ecologists that chaos should be rare in ecological systems. This view nevertheless is not shared by all, e.g., Ref. 15.

[a]Electronic mail: bdeng@math.unl.edu
[b]Electronic mail: ghines@math.unl.edu

The current state of research seems to lead to the question of why food chain chaos is so rare in the field? Although there are some working hypotheses based on the illuminating logistic map,[2] we believe the question cannot be adequately addressed until most, if not all, chaos generating mechanisms are properly categorized and understood for food chain models.

It is with this in mind that a program was initiated in Ref. 16 to categorize chaos generating mechanisms in food chain models. Conditions were found in Ref. 16 for the first of four chaos mechanisms proposed. The mechanism analyzed in that paper is due to the existence of a junction-fold point.[17–19] It was demonstrated rigorously for the first time that the period-doubling cascade to a Rössler-type attractor existed in a food chain model. The second installment[20] identified another set of conditions under which the model admits a Shilnikov saddle-focus homoclinic orbit. The mechanism by which such an orbit appears is due to the existence of a singular counterpart that was analyzed theoretically in Ref. 21 and applied to a physical model for the first time in Ref. 20.

This paper is the third installment in the series, with the intent to unveil a new chaos generating mechanism. This mechanism is not related to Rössler-type attractors or to Shilnikov orbits, two of the most predominant chaos generating mechanisms in mathematical models. Before this, it was unknown even in abstract settings. The primary cause is due to the existence of transcritical points which appear naturally in the class of food chain models with Holling Type II predators, which we consider here. Such points lead to the phenomenon known in the theory of singular perturbation as *Pontryagin's delay of loss of stability*.[22–24] We will prove that it is because of this delayed stability loss that the model admits a set of orbits conjugate to the shift dynamics on two symbols. The parameter region for which this result holds will be given specifically in the main result of the paper, Theorem 4.1.

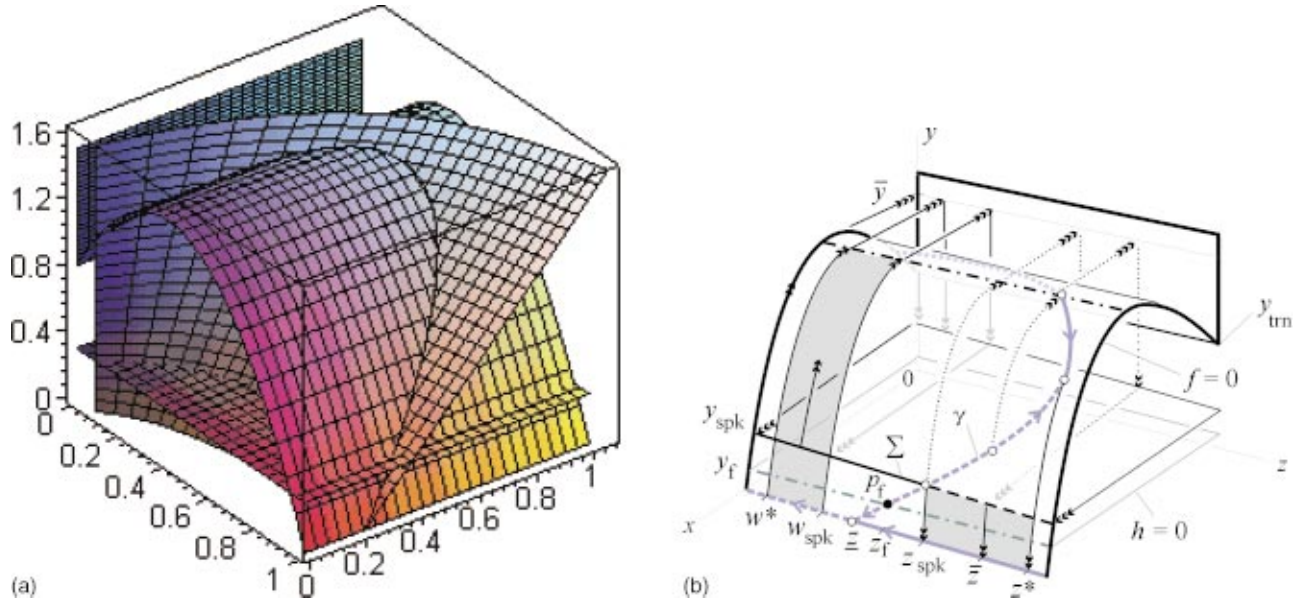

FIG. 1. (Color) (a) Part of the x-nullcline surface $\{x=0, y \geqslant y_{trn}\} \cup \{f(x,y)=0\}$; the nontrivial y-nullcline $\{g(x,y,z)=0\}$; and the nontrivial z-nullcline $\{y=y_f\}$. (b) Geometric illustration for the nullclines and parametrized variables.

II. PRELIMINARY ANALYSIS

We continue to consider the following Rosenzweig-MacArthur model[25] for food chains analyzed in Refs. 16 and 20:

$$\dot{x}=x\left(r-\frac{rx}{K}-\frac{p_1 y}{H_1+x}\right),$$
$$\dot{y}=y\left(\frac{c_1 x}{H_1+x}-d_1-\frac{p_2 z}{H_2+y}\right), \tag{2.1}$$
$$\dot{z}=z\left(\frac{c_2 y}{H_2+y}-d_2\right),$$

with a logistic prey (x), a Holloing type II predator (y), and a Holling type II top-predator (z).[26] With the following changes of variables and parameters first used in Ref. 16:

$$t\to c_1 t, \quad x\to\frac{1}{K}x, \quad y\to\frac{p_1}{rK}y, \quad z\to\frac{p_2 p_1}{c_1 rK}z,$$
$$\zeta=\frac{c_1}{r}, \quad \varepsilon=\frac{c_2}{c_1}, \quad \beta_1=\frac{H_1}{K}, \quad \beta_2=\frac{H_2}{Y_0} \tag{2.2}$$
$$\text{with } Y_0=\frac{rK}{p_1}, \quad \delta_1=\frac{d_1}{c_1}, \quad \delta_2=\frac{d_2}{c_2},$$

Eq. (2.1) is changed to the following dimensionless form:

$$\zeta\dot{x}=x\left(1-x-\frac{y}{\beta_1+x}\right)\coloneqq xf(x,y),$$
$$\dot{y}=y\left(\frac{x}{\beta_1+x}-\delta_1-\frac{z}{\beta_2+y}\right)\coloneqq yg(x,y,z), \tag{2.3}$$
$$\dot{z}=\varepsilon z\left(\frac{y}{\beta_2+y}-\delta_2\right)\coloneqq \varepsilon z h(y).$$

Under the drastic trophic time diversification hypothesis[15] that *the maximum per-capita growth rate decreases from bottom to top along the food chain*, namely

$$r\gg c_1\gg c_2>0 \text{ or equivalently } 0<\zeta\ll 1 \text{ and } 0<\varepsilon\ll 1.$$

Equation (2.3) becomes a singularly perturbed system of three time scales, with the rates of change for the dimensionless prey, predator, and top-predator ranging from fast to intermediate to slow, respectively. We refer to Ref. 16 for the arguments that lead to the scaling above.

Geometric theory of singular perturbation thus is readily applicable to the resulting three-time scale model Eq. (2.3). In particular, nullcline analysis will be used extensively throughout. Nullclines are surfaces along which one of the derivatives is 0. The x-nullcline ($\dot{x}=0$) consists of two smooth surfaces: the trivial branch $x=0$, and the nontrivial branch $f(x,y)=0$ on which we can solve for y as a quadratic function $y=\phi(x)=(1-x)(\beta_1+x)$. The graph of the nontrivial branch is the parabolic surface shown in Fig. 1 and the fold is given by $(\bar{x},\bar{y})$, also the maximum point of $y=\phi(x)$, where $\bar{x}=(1-\beta_1)/2, \bar{y}=(1+\beta_1)^2/4$. These two branches of x-nullclines meet along the line $\{x=0, y=y_{trn}\}, y_{trn}=\beta_1$, consisting of the so-called *transcritical points* which are double zero points for $\dot{x}$.

Similarly, the y-nullcline ($\dot{y}=0$) consists of two surfaces: the trivial one, $y=0$, and the nontrivial one $g(x,y,z)=0$, shown in full in Fig. 1(a). The intersection of $g=0$ and $f=0$ is a curve on the face of the parabola, denoted by γ in Fig. 1(b). The intersection of the parabola fold $\{x=\bar{x}, y=\bar{y}\}$ with the y-nullcline is the point $(\bar{x},\bar{y},\bar{z})=\gamma\cap\{x=\bar{x}, y=\bar{y}\}$. The intersection of the trivial y-nullcline with the nontrivial x-nullcline is the line $\{x=1, y=0\}$ on the parabola. More importantly, on the nontrivial x-nullcline, the trivial y-nullcline ($y=0$) and and nontrivial y-nullclines (γ) intersect at $(1,0,\underline{z})$. This is a transcritical point for the y equation.

It is the existence of this point that leads to the chaos generation mechanism that we are considering in this paper.

The z-nullcline consists of the trivial nullcline $z=0$ and the plane $h(y)=0$ parallel to the xz plane. We denote the value of y on this plane by $y=y_f$, where $y_f=\beta_2\delta_2/(1-\delta_2)$. The intersection of the three nontrivial nullclines of the prey, predator, and the top-predator gives the nontrivial equilibrium point, $p_f(x_f,y_f,z_f)=\{y=y_f\}\cap\gamma$. This point is stable iff it lies on the solid part of γ between the x-nullcline fold point $(\overline{x},\overline{y},\overline{z})$ and the y-nullcline fold point (x^*,y^*,z^*) at which γ is maximum in the variable z. If it lies below $y=y^*$ it is unstable.

Orbits traveling downwards along the trivial nullcline $x=0$ will leave the nullcline at points $y_{\rm spk}(z)$ determined by Pontryagin's delay of loss of stability.[16,22,23,27,28] The value of such a point is determined by the integral

$$\int_{y_{\rm spk}}^{\overline{y}}\frac{f(0,\xi)}{\xi g(0,\xi,z)}d\xi=0. \tag{2.4}$$

Let $p_{\rm spk}=(x_{\rm spk},y_{\rm spk},z_{\rm spk})$ be the intersection of the planar surface $y=y_{\rm spk}(z)$ with the curve γ as depicted in Fig. 1(b). Deng[15] proves that under the condition $z_{\rm spk}<\overline{z}$, which must hold in a certain domain of the original parameter space, a period-doubling cascade to chaos must take place as the nontrivial z-nullcline plane $y=y_f$ crosses the point $p_{\rm spk}$ from above for sufficiently small $0<\varepsilon\ll 1$ and $\zeta=0$. This scenario persists to some extent for sufficiently small $0<\zeta\ll 1$.

The work in Ref. 20 demonstrates instead that the nontrivial equilibrium point p_f must become an unstable spiral if ε increases beyond a modest value ε_0. This occurs in another domain of the original parameter space. When coupled with the same condition that $z_{\rm spk}<\overline{z}$, it is proven that at the point where p_f crosses $p_{\rm spk}$, a singular Shilnikov saddle-focus homoclinic orbit[2] exists for $\zeta=0$ and persists for all sufficiently small $0<\zeta\ll 1$. Chaotic dynamics occur as a result of such orbits.

The parameter constraints under consideration in this paper are the same as in Ref. 16 except that the nontrivial z-nullcline $y=y_f$ lies below the point $p_{\rm spk}$ for all z; that is

$$z_f<z_{\rm spk}<\overline{z},\quad 0<\varepsilon\ll 1,\quad 0<\zeta\ll 1. \tag{2.5}$$

III. SINGULAR PERTURBATION

The dimensionless system (2.3) with singular parameters $0<\varepsilon\ll 1, 0<\zeta\ll 1$ permits a singular perturbation approach.[17,21,29–32] The key is to construct a full picture of the three-dimensional system by piecing together lower dimensional systems obtained at the singular limits when either $\zeta=0$, $\varepsilon=0$ or both.

Fast-intermediate prey-predator dynamics. When Eq. (2.3) is viewed as a singularly perturbed system in ε, the z dynamics are ε-slow and the xy dynamics are ε-fast. More specifically, setting $\varepsilon=0$ gives rise to the ε-fast xy subsystem

$$\begin{aligned}\zeta\dot{x}&=xf(x,y)=x\left(1-x-\frac{y}{\beta_1+x}\right),\\ \dot{y}&=yg(x,y,z)=y\left(\frac{x}{\beta_1+x}-\delta_1-\frac{1}{\beta_2+y}z\right),\\ \dot{z}&=0.\end{aligned} \tag{3.1}$$

It is a two-dimensional system in variables x and y, parametrized by z. Its phase portrait, for fixed z, can be easily constructed from the x- and y-nullclines. To do this, we again treat Eq. (3.1) as a singularly perturbed system, this time using $0<\zeta\ll 1$ as the singular parameter. The variable x is ζ-fast and the variable y is ζ-slow. Specifically, if we rescale the time $t\to t/\zeta$ for Eq. (3.1) and set $\zeta=0$, then we obtain its ζ-fast subsystem

$$x'=xf(x,y),\quad y'=0,\quad z'=0.$$

It is one-dimensional in x with both y and z being frozen parameters. Its flow is completely determined by the equilibrium surface $xf(x,y)=0$. Of the x-nullcline surfaces only two branches are attracting. These are $\{x=0,y>\beta_1\}$ and $\{f=0,\overline{x}<x\leqslant 1\}$.

Setting $\zeta=0$ in Eq. (3.1) gives rise to the intermediate, ζ-slow subsystem in y:

$$0=xf(x,y),\quad \dot{y}=yg(x,yz)=y\left(1-x-\frac{y}{\beta_1+x}\right),\quad \dot{z}=0.$$

Its flow is restricted to the x-nullcline surfaces $x=0$ and $f(x,y)=0$, and determined by the y-nullcline $y=0$ and $g(x,y,z)=0$. Above the nontrivial y-nullcline $g(x,y,z)=0$, we have $\dot{y}>0$, and so $y(t)$ increases. Below it, $\dot{y}<0$ and $y(t)$ decreases.

Putting together the flows for the two subsystems, we get the phase portrait for Eq. (3.1) which is shown in Fig. 2 and Fig. 1(b).

Intermediate-slow predator-superpredator dynamics. In Eq. (2.3), x evolves on the fastest time scale. In a perturbed state with $0<\zeta\ll 1$, all solutions are quickly attracted to a branch of the x-nullcline: either $\{x=0,y>\beta_1\}$ or $\{f=0,x>\overline{x}\}$ because the rate of change for x is much greater than that of y and z if their initial points are not already near these surfaces. In a sufficiently small neighborhood of the surfaces, solutions are well approximated by the reduced ζ-slow flows by setting $\zeta=0$ in Eq. (2.3),

$$xf(x,y)=0,\ \dot{y}=yg(x,y,z),\quad \dot{z}=\varepsilon zh(y).$$

This is a two-dimensional system in y and z restricted to either $x=0$ or $\{f(x,y)=0\}$.

The yz dynamics is rather simple on $x=0$. In fact, the reduced yz equations are

$$\begin{aligned}\dot{y}&=yg(0,y,z)=y\left(-\delta_1-\frac{1}{\beta_2+y}z\right)<0,\\ \dot{z}&=\varepsilon zh(y)=\varepsilon z\left(\frac{y}{\beta_2+y}-\delta_2\right).\end{aligned}$$

Hence all solutions develop downward toward $y=0$. They will cross the transcritical line $y=y_{\rm trn}=\beta_1$ and jump to the stable branch of the nontrivial x-nullcline $f(x,y)=0$ at the Pontryagin turning point $y=y_{\rm spk}(z)$ as noted earlier. We point out that it is proved in Ref. 28 that $y=y_{\rm spk}(z)$ defined

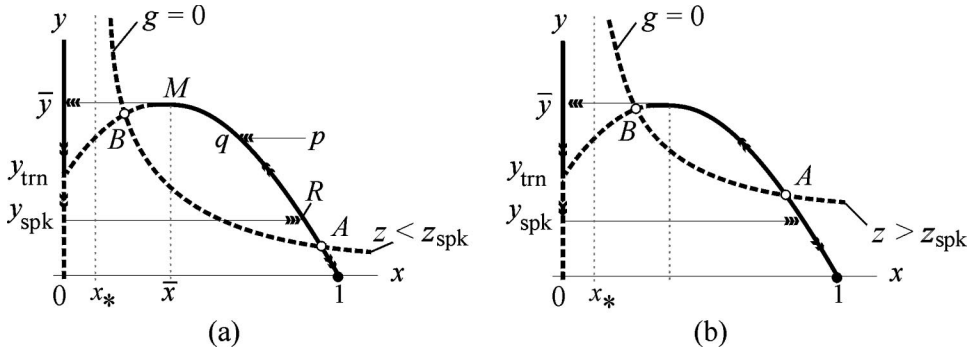

FIG. 2. Phase portraits of the ε-fast subsystem in x,y with $\zeta=0$. (a) A specific value of z with $0<z<z_{\text{spk}}$ and (b) several typical values of z. In (a) the ζ-fast x-flow lines are parallel to the x axis. The ζ-slow y flows are on the x-nullcline surfaces $x=0$ and $f(x,y)=0$, oriented by double arrow heads. Points A,B are equilibrium points. All nonequilibrium singular orbits are attracted to either the relaxation cycle $M\bar{y}_{\text{spk}}R$ or the steady state $(x,y)=(1,0)$ for $z<z_{\text{spk}}$. The turning point y_{spk} is determined by the integral equation (2.4) of Pontryagin's delay of stability loss. In (b) the singular relaxation cycle becomes a singular homoclinic orbit at $z=z_{\text{spk}}$, and disappears for $z>z_{\text{spk}}$. For $z<\bar{z}$, equilibrium points A, B are unstable. For $\bar{z}<z<z^*$, B is stable and A is unstable. Both disappear for $z>z^*$. The equilibrium point (1,0) is always attracting, locally, and globally for $z>z_{\text{spk}}$. A three-dimensional view of these portraits in terms of z cross sections is referred to Fig. 1(b).

by Eq. (2.4) is a monotone decreasing function in z. Σ is the horizontal projection of the Pontryagin turning curve $y=y_{\text{spk}}(z)$ onto the nontrivial x-attracting surface $\{f(x,y)=0,x>\bar{x}\}$.

The yz dynamics on the nontrivial and stable x-nullcline branch $\{f(x,y)=0,x>\bar{x}\}$ is a little bit more complex, and determines the chaotic behavior we will describe later. Given $0\leqslant y\leqslant\bar{y}$, define $x=\psi(y)$ to be the value of x in $[\bar{x},1]$ such that (x,y) lies on the stable branch of $f(x,y)=0$; that is $f(\psi(y),y)=0,0\leqslant y\leqslant\bar{y}$. Then the reduced yz equations are

$$\dot{y}=yg(\psi(y),y,z)=y\left(\frac{\psi(y)}{\beta_1+\psi(y)}-\delta_1-\frac{1}{\beta_2+y}z\right),$$
$$\dot{z}=\varepsilon zh(y)=\varepsilon z\left(\frac{y}{\beta_2+y}-\delta_2\right). \tag{3.2}$$

It is again a two-dimensional singularly perturbed system with singular parameter ε. The y equation is ε-fast. The z equation is ε-slow and is restricted to the y-nullcline. Similar to the analysis for the ζ-fast xy subsystem, the dynamics are essentially determined by the y-nullcline $\{y=0\}$, $\{g(x,y,z)=0\}$ and the z-nullcline $\{z=0\}$, $\{h(y)=0\}$. The two trivial nullclines, $\{y=0\}$ and $\{z=0\}$ are invariant and the dynamics on them are simple. The nontrivial y-nullcline restricted to $\{f(x,y)=0,x>\bar{x}\}$ is the curve $\gamma=\{g(x,y,z)=0\}\cap\{f(x,y)=0,x>\bar{x}\}$ introduced earlier. The nontrivial z-nullcline $h(y)=0$ on which $y=y_f=\beta_2\delta_2/(1-\delta_2)$. Two phase plane portraits are illustrated in Figs. 3(a) and 3(b).

Most important, the point $(1,0,\underline{z})$ or $\underline{z}$ as shown in Fig. 3 is a transcritical point for Eq. (3.2) and the phenomenon of Pontryagin's delay of loss of stability occurs, now for the yz

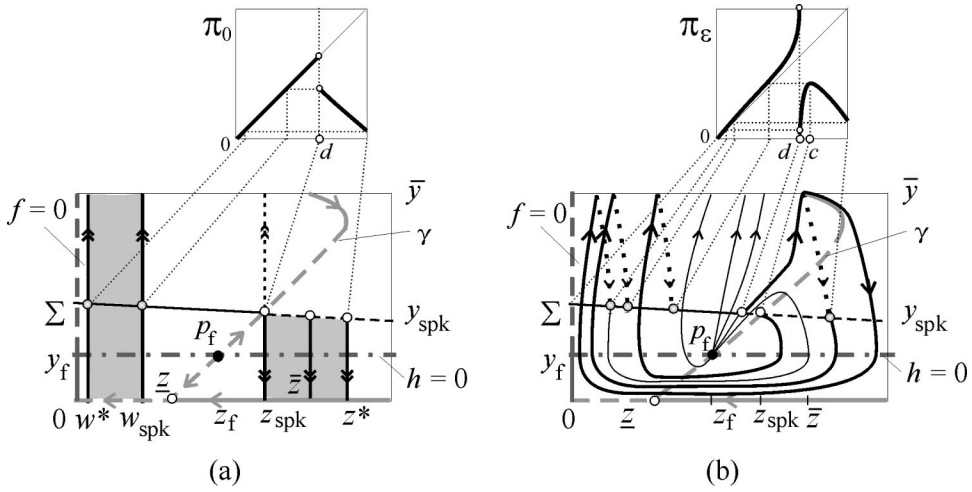

FIG. 3. Phase portraits of the yz subsystems on the stable branch of the nontrivial x-nullcline $\{f(x,y)=0\}$ and the corresponding singular return maps for $\zeta=0$. (a) The case with $\varepsilon=0$. On dashed parts of the y-nullclines, the equilibria are repelling. On solid parts, they are attracting. The ε-fast flows develop vertically and are shown with double arrows. Upon rescaling $t\to\varepsilon t$ and setting $\varepsilon=0$ in Eq. (3.2), it gives rise to the ε-slow subsystem in z restricted on the y-nullclines $y=0$ and γ. For points above the z-nullcline $y=y_f$, z increases; and for points below it, z decreases. The oriented parts of the y-nullclines with single arrows are the reduced ε-slow flowlines. (b) The return map at perturbed state $0<\varepsilon\ll 1$. Dotted single-arrowed curves are the yz flowlines on the trivial x-nullcline $x=0$. See the text for description.

flow. The theory again applies. In particular, let (y,z) be any point on Σ, for example, right of z_{spk}. The perturbed flow (with $0<\varepsilon\ll 1$ in Eqs. (3.2)) through (y,z) moves down and to the right, following the vector field. It crosses the z-nullcline $y=y_f$ vertically and then moves left and still down. It crosses γ horizontally and then moves up and still left. It crosses $y=y_f$ vertically. From there it continues to the right and still up, and hits the junction curve Σ at a point denoted by $(v_\varepsilon(z),w_\varepsilon(z))$. This defines a diffeomorphism from z to $w_\varepsilon(z)$. Pontryagin's theory implies that $\lim_{\varepsilon\to 0} w_\varepsilon(z)=w(z)$ exists and $w(z)$ is determined by the following integral

$$\int_z^w \frac{g(1,0,s)}{sh(0)}\,ds=0. \tag{3.3}$$

Again, the relationship between z and $w(z)$ is diffeomorphic.[20–22] More specifically, by simplifying the integral equation, we find that z and w satisfy the equation $z\exp(-z/\underline{z})=w\exp(-w/\underline{z})$. Because the function $y=x\times\exp(-x/\underline{z})$ increases in $(0,\underline{z}]$ and decreases in $[\underline{z},\infty)$, covering the same range $(0,\underline{z}/e]$, the correspondence between z and w is indeed diffeomorphic. In particular, if we consider the shaded region in Fig. 3(a) bounded by points z_{spk} and z^*, then each vertical segment of the flow in this region corresponds to a unique vertical flow segment in the shaded region bounded by w^* and w_{spk}. This pair of vertical segments together with the ε-slow horizontal flowline from z to w along $\{x=1,y=0\}$ form the singular orbit for an initial condition below the γ curve.

IV. RETURN MAPS AND CHAOS

We now describe the singular orbits of the full system Eq. (2.3) for $\zeta=0$ and $0<\varepsilon\ll 1$. In particular, we only consider initial points on the junction curve Σ. Any typical orbit from Σ will eventually hit the parabola fold $x=\overline{x},y=\overline{y}$ because $z_{\text{spk}}<\overline{z}$ and ε is small. Once the orbit hits the fold, it will jump to the trivial x-nullcline $x=0$, move down along $x=0$, jump back to Σ at $y=y_{\text{spk}}$. This defines the singular Poincaré return map π_ε for $\zeta=0$. Note that the image of π_ε is the point where the orbit hits Σ *after* first visiting $x=0$. So orbits starting on the right side of z_{spk} on Σ will hit Σ exactly once before returning to Σ as the image of the Poincaré map.

One effective way to view this map is by looking directly into the x axis as shown in Fig. 3. The solid oriented curves are the ζ-slow orbits on the attracting branch of the parabola $\{f(x,y)=0,\overline{x}\leqslant x\leqslant 1\}$. The dotted, downward-oriented curves are those on the trivial x-nullcline $x=0$ for $y\geqslant y_{\text{spk}}$. The fast jumps from the fold to the plane $x=0$ as well as from the Pontryagin turning curve $y=y_{\text{spk}}$ to Σ are perpendicular to the projected yz plane, and thus hidden from our view. We now describe in greater detail the singular return map π_ε in this setting.

First, we identify Σ with an interval and the singular return map π_ϵ as an interval map, depicted in Fig. 3(b). There are two special points on Σ that are essential to the definition of π_ϵ. The first point, labeled as d, corresponds to the unique point on Σ for which the orbit [of Eq. (3.2)] passing through it intersects the fold at $(\overline{x},\overline{y},\overline{z})$. From this point, the orbit can either jump to the $x=0$ plane or stay on the nullcline $f=0$ and pass horizontally through γ. In the first case, the orbit travels down $x=0$ and jumps back to Σ. The point it hits Σ is denoted by $z_\varepsilon^*=\pi_\varepsilon(d)$, which we will take to be the rightmost end point of the interval of definition of π_ε. In the second case, the orbit comes down and intersects Σ at a point far right of $\overline{z}$. It then goes around p_f, up to the fold, down $x=0$ and returns to Σ at a point, denoted by w_ε^*, near $z=0$. This point marks the left end point of the interval. Notice that d divides Σ into two subintervals, the left and right intervals. On the left interval, π_ε is strictly increasing and its graph lies above the diagonal. This is because the left interval lies above the z-nullcline $y=y_f$ and the z-component of the singular orbit increases. The second special point, denoted by c, corresponds to a junction-fold point[10] where Σ is tangent to the ζ-slow vector field on the parabola $\{f=0,\overline{x}<x\}$ for $0<\varepsilon\ll 1$. (If Σ is parallel to the z axis, which is the case when $\delta_1=0$, then c is the point of intersection of the y-nullcline curve γ with Σ. If Σ is monotone decreasing in z, the point c lies to the right of the intersection.) For any initial condition on Σ to the right of c, the singular orbit swings down and around p_f before hitting the fold $y=\overline{y}$. From there it jumps to $x=0$ and then eventually returns to Σ. (The first hit on Σ is not the *returning* hit because it has not visited the trivial x-nullcline $x=0$ yet.) For initial conditions on Σ between d and c, the orbit crosses γ after moving above c, develops downward, goes around p_f, moves up to the fold, jumps to $x=0$, and eventually returns to Σ. The image of the interval $[d,c]$ is $[w_\varepsilon^*,\pi_\varepsilon(c)]$ and the image of the interval $[c,z_\varepsilon^*]$ is $[\pi_\varepsilon(c),\pi_\varepsilon(z_\varepsilon^*)]$. π_ε has a local maximum at the junction-fold point c. It is monotone increasing in the interval $[d,c]$ and monotone decreasing in the interval $[c,z_\varepsilon^*]$.

What makes the return map π_ε potentially chaotic is the existence of the transcritical point $\underline{z}$. As $\varepsilon\to 0$, $\pi_0=\lim \pi_\varepsilon$ exists. More specifically, points d and c collapse to one point, denoted by d in Fig. 3(a). The graph on the left interval converges to the diagonal. The graph right of c converges to a *strictly* decreasing curve determined diffeomorphically by the Pontryagin integral (3.3), see also Figs. 3(a) and 1(b). As a result, the length of the interval $[\pi_0(c),\pi_0(z^*)]$ must be nonzero. We call this length η_0. It is because of this property and the property that the return map's graph on the left interval collapses down to the diagonal at $\varepsilon=0$ that π_ε must be chaotic for sufficiently small $0<\varepsilon\ll 1$.

There are several ways to demonstrate the chaos. We present one argument here. Let $I_0=(d,z_\varepsilon^*]$ be the right interval of Σ, and $I_n=\pi_\varepsilon^{-n}(I_0)\cap[0,d]$. I_n is the part of the nth pre-image of I_0 that is in the left interval. See Fig. 4 for an illustration. Define the end points $d_0=d$ and $d_n=\pi_\varepsilon^{-1}(d_{n-1})$ so that $I_n=(d_n,d_{n-1}]$. We know each d_n exists because of the monotonicity of π_ε on $(0,d]$ and the fact that $\pi_\varepsilon(0)=0$. The nth image of I_n under π_ε is I_0 and so, under one more iteration, the graph of $\pi_\varepsilon^{n+1}|_{I_n}$ is a unimodal map similar to $\pi_\varepsilon|_{I_0}$ with the same values at the end points and the same maximum value. In Fig. 4(b), graphs are shown for $\pi_\varepsilon^2|_{I_1}$, $\pi_\varepsilon^3|_{I_z}$, and $\pi_\varepsilon^{n+1}|_{I_n}$.

To see why π_ε is chaotic, choose n so that d_{n+1}

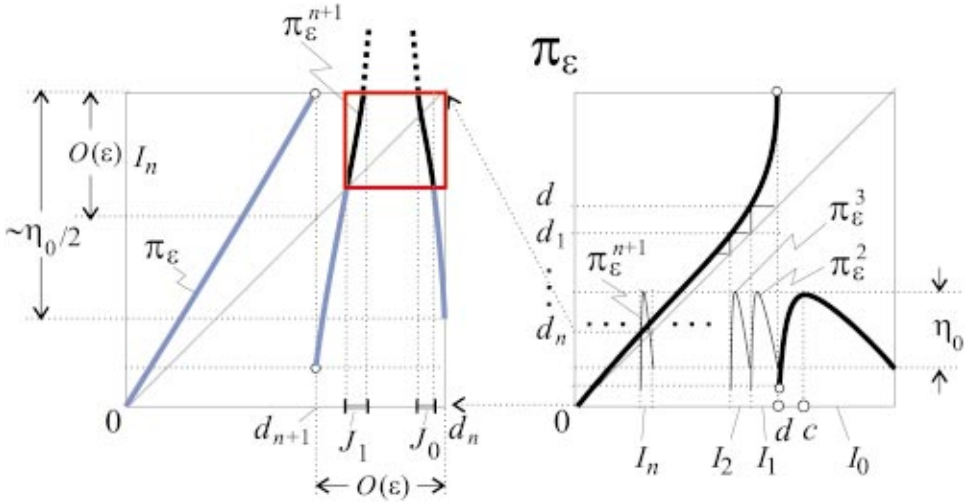

FIG. 4. (Color) Symbolic dynamics on two symbols follows when π_ε^{n+1} is restricted to the upper right corner box (red) in the interval $I_n=(d_{n+1},d_n]$.

$\leqslant \pi_\varepsilon(c)-\eta_0/2<d_n$ and zoom in on the interval I_n as shown in Fig. 4. Because the graph of π_ε on the left interval $[0,d)$ collapses onto the diagonal as $\varepsilon\to 0$, the length of I_n must be order $O(\varepsilon)$. On the other hand, by the choice of n, the image $\pi_\varepsilon^{n+1}(I_n)$ of I_n must cover an interval of length at least $\eta_0/2>0$, thus it must cover I_n, i.e., $\pi_\varepsilon^{n+1}(I_n)\supset I_n$. In Fig. 4(a), we blow up the picture in Fig. 4(b) on the interval $[0,d_n]$. In this picture, we can see part of π_ε and $\pi_\varepsilon^{n+1}|_{I_n}$.

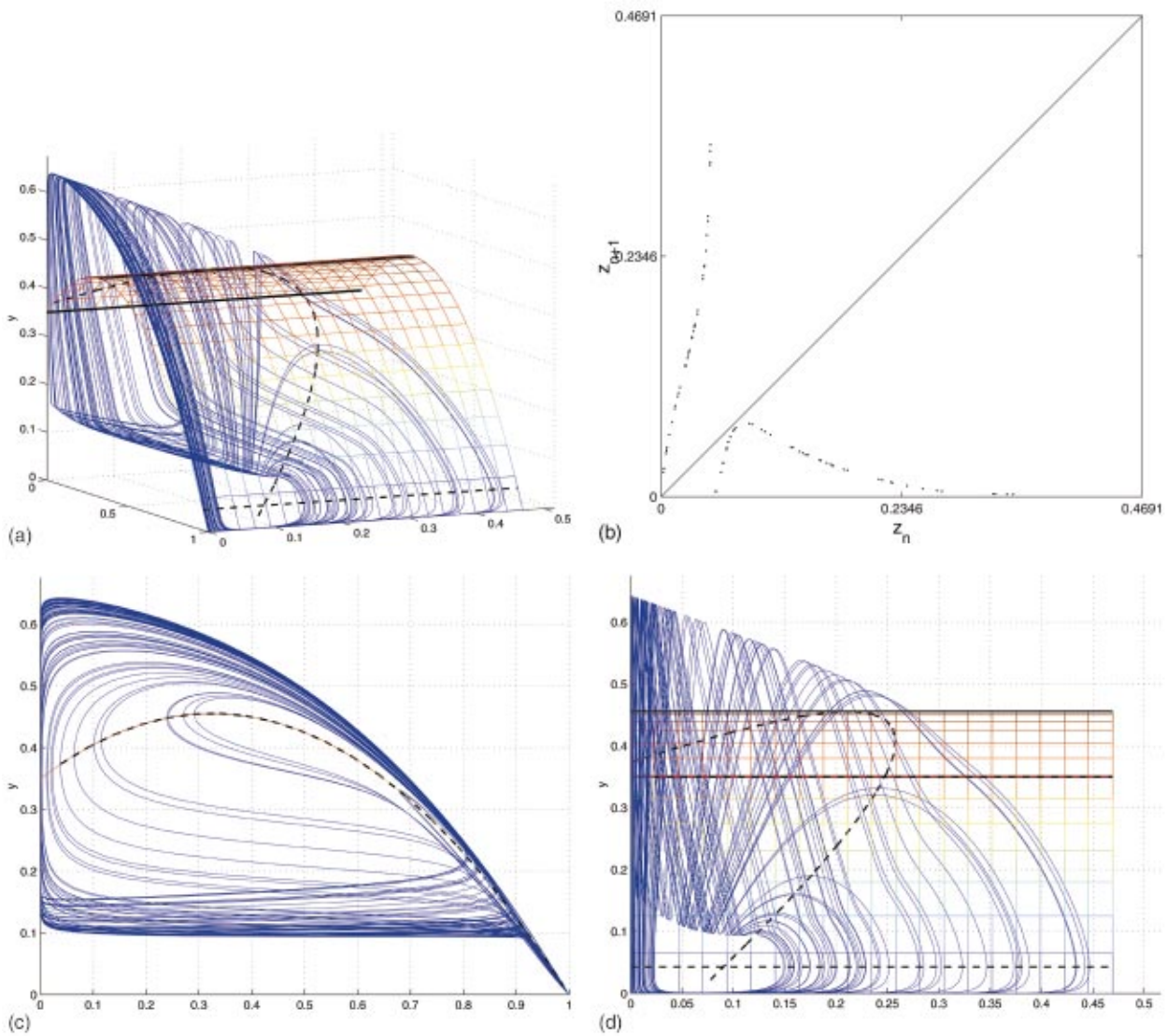

FIG. 5. (Color) Numerical simulation with parameter values $\zeta=0.1$, $\varepsilon=0.34$, $\beta_1=0.35$, $\beta_2=0.1$, $\delta_1=0.1$, $\delta_2=0.3$. (a) A three-dimensional view. (b) A Poincaré return map. (c) Projected on to the xy plane. (d) Projected on the zy plane (z axis horizontal).

We also mark I_n on the vertical axis so that we can see $I_n \subset \pi_\varepsilon^{n+1}(I_n)$ easily. We can further restrict π_ε^{n+1} to the box in the upper right corner. We define J_0, J_1 to be two disjoint closed interval pre-images of the part of the graph in the box. This implies immediately,[33] that there is a Cantor subset $\Omega \subset J_0 \cup J_1$ on which the dynamics of π_ε^{n+1} is conjugate to the shift dynamics on two symbols: $.s_0 s_1 \cdots \mapsto .s_1 s_2 \cdots$ with $s_i \in \{J_0, J_1\}$. Therefore, we have proved the following theorem.

Theorem 4.1: *Under the conditions that* $\underline{z} < z_f < z_{\text{spk}} < \overline{z}$ *and* $\zeta = 0$, *the singular Poincaré return map* π_ε *for every sufficiently small* $0 < \varepsilon \ll 1$ *has a subset on which* π_ε^{n+1} *is conjugate to the shift map on two symbols.*

Guided by the conditions of Eq. (2.5), a perturbed attractor was numerically found and shown in Fig. 5.

V. CLOSING REMARKS

We have demonstrated that in a certain parameter range, the food chain model (2.1) must have a chaotic invariant set on which the shift dynamics on two symbols can be embedded. This phenomenon is due to the existence of a transcritical point for the predator-superpredator interaction. Without such a point, the graph of the Poincaré return map π_ε over the right interval $(d,b]$ may lay flat at the singular limit $\varepsilon = 0$ which is the case at a fold turning point.[8] When such is the case, the argument for the existence of symbolic dynamics does not apply.

We have left open the question of whether or not this chaotic set is part of a strange attractor. This question cannot be answered without further partitioning the parameter space. This is because the return map could have a superstable periodic orbit if the critical point of the graph over some interval I_m happens to cross the diagonal. We also left open the question of whether the Lyapunov exponents of the orbits found in Theorem 4.1 are greater than 0. We strongly believe this is the case. One formal argument follows this line of reasoning. At the limit $\varepsilon \to 0$, the graph of π_ε^{n+1} over the interval I_n becomes vertical while that over the left interval, $[0,d)$, collapses onto the diagonal and that over the right interval, $(d,z^*]$, becomes strictly decreasing. Thus for sufficiently small $0 < \varepsilon \ll 1$, the slopes of the graphs of π_ε^{n+1} over the subintervals $J_0, J_1 \subset I_n$ are strictly greater than 1, implying that all Lyapunov exponents are greater than 0. We have also left open the persistence question, that of whether or not part of the chaotic dynamics persists when the system is perturbed by $0 < \zeta \ll 1$. This question is closely related to the last one. The structure must persist if one can show it is hyperbolic.

In relation to the other two mechanisms analyzed in Refs. 15 and 19, we point out that as y_f increases and crosses y_{spk}, the transcritical chaos generating mechanism changes to the junction-fold mechanism.[15] With increasing ε, the transcritical chaos generating mechanism then gives way to the Shilnikov mechanism.[19] We will examine the role these different types of chaos play in questions regarding chaos in ecology after most and enough, if not all, chaos generation mechanisms are categorized for the food chain model Eq. (2.1).

[1] R. May, ''Simple mathematical models with very complicated dynamics,'' Nature (London) **261**, 459–467 (1976).
[2] A. A. Berryman and J. A. Millstein, ''Are ecological systems chaotic—and if not, why not?'' Trends Ecol. Evol. **4**, 26–28 (1989).
[3] S. Ellner and P. Turchin, ''Chaos in a noisy world: New methods and evidence from time-series analysis,'' Am. Nat. **145**, 343–375 (1995).
[4] V. Rai and W. M. Schaffer, ''Chaos in ecology,'' Chaos, Solitons Fractals **12**, 197–203 (2001).
[5] R. F. Costantino, J. M. Cushing, B. Dennis, and R. A. Desharnais, ''Experimentally induced transitions in the dynamics behavior of insect populations,'' Nature (London) **375**, 227–230 (1995).
[6] P. Hogeweg and B. Hesper, ''Interactive instruction on population interactions,'' Comput. Biol. Med. **8**, 319–327 (1978).
[7] M. E. Gilpin, ''Spiral chaos in a predator-prey model,'' Am. Nat. **113**, 306–308 (1979).
[8] O. E. Rössler, ''Chaotic behavior in simple reaction systems,'' Z. Naturforsch. A **31**, 259–264 (1976).
[9] A. Hastings and T. Powell, ''Chaos in a three-species food chain,'' Ecology **72**, 896–903 (1991).
[10] H. L. Smith and P. Waltman, ''The theory of the Chemostat—Dynamics of microbial competition,'' *Cambridge Studies in Mathematical Biology* (Cambridge University Press, Cambridge, 1994).
[11] L. P. Sil'nikov, ''A case of the existence of a denumerable set of periodic motions,'' Sov. Math. Dokl. **6**, 163–166 (1965).
[12] K. McCann and P. Yodzis, ''Bifurcation structure of a three-species food chain model,'' Theor. Popul. Biol. **48**, 93–125 (1995).
[13] Y. A. Kuznetsov, O. De Feo, and S. Rinaldi, ''Belyakov homoclinic bifurcations in a tritrophic food chain model,'' SIAM (Soc. Ind. Appl. Math.) J. Appl. Math. **62**, 462–487 (2001).
[14] Yu. A. Kuznetsov and S. Rinaldi, ''Remarks on food chain dynamics,'' Math. Biosci. **133**, 1–33 (1996).
[15] B. Blasius, A. Huppert, and L. Stone, ''Complex dynamics and phase synchronization in spatially extended ecological systems,'' Nature (London) **399**, 354–359 (1999).
[16] B. Deng, ''Food chain chaos due to junction-fold point,'' Chaos **11**, 514–525 (2001).
[17] B. Deng, ''Constructing homoclinic orbits and chaotic attractors,'' Int. J. Bifurcation Chaos Appl. Sci. Eng. **4**, 823–841 (1994).
[18] B. Deng, *Folding at the Genesis of Chaos*, Proceedings of the First World Congress of Nonlinear Analysts (de Gruyter, Berlin, 1996), Vol. III, pp. 3765–3777.
[19] B. Deng, ''Glucose-induced period-doubling cascade in the electrical activity of pancreatic β-cells,'' J. Math. Biol. **38**, 21–78 (1999).
[20] B. Deng and G. Hines, ''Food chain chaos due to Shilnikov's orbit,'' Chaos **12**, 533–538 (2002).
[21] K. Taylor and B. Deng, ''Chaotic attractors in one-dimension generated by a singular Shilnikov orbit,'' Int. J. Bifurcation Chaos Appl. Sci. Eng. **12**, 3059–3083 (2001).
[22] S. Schecter, ''Persistent unstable equilibria and closed orbits of a singularly perturbed equation,'' J. Diff. Eqns. **60**, 131–141 (1985).
[23] E. F. Mishchenko, Yu. S. Kolesov, A. Yu. Kolesov, and N. Kh. Rozov, *Asymptotic Methods in Singularly Perturbed Systems, Monographs in Contemporary Mathematics* (Consultants Bureau, New York, 1994).
[24] W. Liu, ''Exchange lemmas for singularly perturbed problems with certain turning points,'' J. Diff. Eqns. **167**, 134–180 (2000).
[25] M. L. Rósenzweig and R. H. MacArthur, ''Graphical representation and stability conditions of predator-prey interactions,'' Am. Nat. **97**, 209–223 (1963).
[26] C. S. Holling, ''Some characteristics of simple types of predation and parasitism,'' Canadian Entomologist **91**, 385–398 (1959).
[27] L. C. Pontryagin, ''Asymptotic behavior of solutions of systems of differential equations with a small parameter at higher derivatives,'' Izv. Akad. Nauk. SSSR Ser. Math. **21**, 605–626 (1957) (in Russian).
[28] S. Rinaldi and S. Muratori, ''Slow-fast limit cycles in predator-prey models,'' Ecol. Modell. **61**, 287–308 (1992).
[29] S. Muratori and S. Rinaldi, ''Low- and high-frequency oscillations in three-dimensional food chain system,'' SIAM (Soc. Ind. Appl. Math.) J. Appl. Math. **52**, 1688–1706 (1992).

[30] B. Deng, ''Constructing Lorenz type attractors through singular perturbations,'' Int. J. Bifurcation Chaos Appl. Sci. Eng. **5**, 1633–1642 (1995).
[31] B. Deng, ''Spiral-plus-saddle attractors and elementary mechanisms for chaos generation,'' Int. J. Bifurcation Chaos Appl. Sci. Eng. **6**, 513–527 (1996).
[32] O. De Feo and S. Rinaldi, ''Singular homoclinic bifurcations in tritrophic food chains,'' Math. Biosci. **148**, 7–20 (1998).
[33] T.-Y. Li and J. Yorke, ''Period three implies chaos,'' Am. Math. Monthly **82**, 985–992 (1975).